ELSEVIER

Computational Materials Science 23 (2002) 270–282

COMPUTATIONAL MATERIALS SCIENCE

www.elsevier.com/locate/commatsci

Diffuse-interface modeling of composition evolution in the presence of structural defects

S.Y. Hu, L.Q. Chen *

Department of Materials Science and Engineering, The Pennsylvania State University, University Park, PA 16802, USA

Accepted 1 June 2001

Abstract

A diffuse-interface phase field model is described for modeling the interactions between compositional inhomogeneities and structural defects. The spatial distribution of these structural defects is described by the space-dependent eigenstrains. It takes into account the effect of the coherency elastic energy of a compositional inhomogeneity, and the elastic coupling between the coherency strains and defect strains. The temporal evolution of composition is described by the Cahn–Hilliard equation. Particularly, the solute segregation, and nucleation and growth around dislocation slip bands and crack-like condensed interstitial dislocation loops are discussed. The effect of nucleated coherent precipitates on the stress field around these defects is analyzed

Keywords: Nucleation; Composition segregation; Defects; Phase field; Continuously distributed dislocations; Microstructure

1. Introduction

Many important processes in crystalline solids, such as diffusional phase transformations and microstructure coarsening, involve diffusional redistribution of atoms under the influence of stresses [1–3]. The stresses may arise from, e.g., a composition-dependent lattice parameter, an external field, or the presence of internal structural defects. Recent theoretical and modeling studies have been mainly focused on the effect of coherency stresses due to a composition-dependent lattice parameter, see for example [4–13], and for a rather thorough list of references on this subject, see a recent review [14]. The interactions between dislocations and coherent precipitates were studied by Lee [15] using the discrete atom method (DAM). The dislocation motion in the presence of diffusing solutes were simulated using a Monte Carlo model by Wang et al. [16]. The effect of dislocations on the morphological evolution during spinodal decomposition was investigated by Léonard and Desai [17] who directly introduced the analytical elastic solution of a dislocation into the Cahn–Hilliard equation [18]. Recently, we proposed a continuum diffuse-interface phase

* Corresponding author. Tel.: +1-814-863-8101; fax: +1-814-865-0016.
E-mail address: lqc3@psu.edu (L.Q. Chen).

0927-0256/02/$ - see front matter
PII: S0927-0256(01)00206-3

field model by coupling the Cahn–Hilliard equation with the elastic fields produced from coherent compositional inhomogeneities as well as from structural defects such as dislocations. This model can easily incorporate elastic anisotropy, and allows arbitrary distribution of composition and defects. The unique feature of this model is the fact that the elastic fields from structural defects and coherent compositional inhomogeneity are obtained within exactly the same formulation using the concept of "eigenstrains". Therefore, any structural defects which can be described by eigenstrains can be introduced into the model. In addition, our model can be conveniently extended to describe redistribution of defects such as dislocation motion by coupling the Cahn–Hilliard diffusion equation with the evolution equation for defect movement. The model has been applied successfully to simulating solute atom segregation around a single edge dislocation [19]. An excellent agreement between the simulated and theoretical solute (Cottrell) atmosphere was obtained. The simulation results also demonstrated that dislocation stress field induces nucleation and growth of a coherent precipitate.

It has long been recognized stress concentrations around crystal defects such as grain boundaries, slip bands and cracks can be the origin of new phase nucleation and local phase transitions [20–24]. New phase formation near such defects not only results in a change in material physical properties, but also a redistribution of stress field, hence may result in a remarkable change of the material damage behavior. Many structural defects such as grain boundaries, slip bands and cracks can be described as certain types of distributed dislocations. In this paper, we consider the interactions between a compositional inhomogeneity and arbitrary distributed dislocations. We studied the compositional segregation, and precipitate nucleation and growth near slip bands and dislocation loops. In particular, the effect of dislocation density on compositional segregation and precipitate morphologies as well as the effect of formed coherent precipitates on the defect stress field are studied.

The work to extend the present model to the elastically inhomogeneous systems and to incorporate the redistribution of dislocations under applied and internal stress fields is currently underway.

2. Elastic potential due to coherency stress and defects

We consider a simple binary solid solution with a compositional inhomogeneity described by $X(\boldsymbol{r})$, representing the mole or atom fraction X at position $\boldsymbol{r}$. If we assume that the variation of stress-free lattice parameter, a, with composition obeys the Vegard's law, the local stress-free strain caused by compositional inhomogeneity is given by,

$$\epsilon^{\mathrm{o}}_{ij}(\boldsymbol{r}) = \epsilon_{\mathrm{o}}\delta X(\boldsymbol{r})\delta_{ij}, \tag{1}$$

where $\epsilon_{\mathrm{o}} = \frac{1}{a}\frac{\mathrm{d}a}{\mathrm{d}X}$ is the composition expansion coefficient of lattice parameter, $\delta X(\boldsymbol{r}) = X(\boldsymbol{r}) - X_{\mathrm{o}}$ with X_{o} being the overall composition of the solid solution, and δ_{ij} is the Kronecker–Delta function. Let $\epsilon^{\mathrm{d}}_{ij}(\boldsymbol{r})$ denote the eigenstrain for a general structural defect distribution. Using Kachaturyan–Shatalov (KS) reciprocal space theory [1,25], for a system with both a compositional inhomogeneity by $\delta X(\boldsymbol{r})$ and structural defects described by $\epsilon^{\mathrm{d}}_{ij}(\boldsymbol{r})$, the total elastic energy in the homogeneous modulus approximation is given by [19]

$$\begin{aligned} E = {} & \frac{V}{2}\lambda_{ijkl}\bar{\epsilon}_{ij}\bar{\epsilon}_{kl} + \frac{V}{2}\lambda_{ijkl}\delta_{ij}\delta_{kl}\epsilon^2_{\mathrm{o}}\overline{[\delta X(\boldsymbol{r})]^2} - \frac{1}{2}\int_g \frac{d^3\boldsymbol{g}}{(2\pi)^3} n_i\sigma^{\mathrm{o}}_{ij}\Omega_{jk}(\boldsymbol{n})\sigma^{\mathrm{o}}_{kl}n_l|\delta X(\boldsymbol{g})|^2 \\ & + \frac{V}{2}\lambda_{ijkl}\overline{\epsilon^{\mathrm{d}}_{ij}(\boldsymbol{r})\epsilon^{\mathrm{d}}_{kl}(\boldsymbol{r})} - \frac{1}{2}\int_g \frac{d^3\boldsymbol{g}}{(2\pi)^3} n_i\sigma^{\mathrm{d}}_{ij}(\boldsymbol{g})\Omega_{jk}(\boldsymbol{n})\{\sigma^{\mathrm{d}}_{kl}(\boldsymbol{g})\}^* n_l - V\lambda_{ijkl}\bar{\epsilon}_{ij}\overline{\epsilon^{\mathrm{d}}_{kl}(\boldsymbol{r})} \\ & + V\sigma^{\mathrm{o}}_{ij}\overline{\delta X(\boldsymbol{r})\epsilon^{\mathrm{d}}_{ij}(\boldsymbol{r})} - \int_g \frac{d^3\boldsymbol{g}}{(2\pi)^3} n_i\sigma^{\mathrm{o}}_{ij}\Omega_{jk}(\boldsymbol{n})\sigma^{\mathrm{d}}_{kl}(\boldsymbol{g})n_l\delta X^*(\boldsymbol{g}), \end{aligned} \tag{2}$$

where V is the total volume of the system, λ_{ijkl} are the elastic constants, $\boldsymbol{g}$ is the wave vector, g_i is the ith component of $\boldsymbol{g}$, $\bar{\epsilon}_{ij}$ is the homogeneous strain, $\delta X(\boldsymbol{g})$ and $\epsilon^{\mathrm{d}}_{kl}(\boldsymbol{g})$ are the Fourier transforms of $\delta X(\boldsymbol{r})$ and $\epsilon^{\mathrm{d}}_{kl}(\boldsymbol{r})$, $G_{ik}(\boldsymbol{g})$ is the inverse tensor to $(G^{-1}(\boldsymbol{g}))_{ik} = g^2\lambda^{\mathrm{o}}_{ijkl}n_jn_l = g^2\Omega^{-1}_{ik}(\boldsymbol{n})$ with $\boldsymbol{n} = \boldsymbol{g}/|g|$, $\sigma^{\mathrm{o}}_{ij} = \lambda_{ijkl}\epsilon_{\mathrm{o}}\delta_{kl}$, $\sigma^{\mathrm{d}}_{ij}(\boldsymbol{g}) = \lambda_{ijkl}\epsilon^{\mathrm{d}}_{kl}(\boldsymbol{g})$. $\overline{\cdots}$ represents the average of the quantity $\cdots$ over the entire volume, and $\{\cdots\}^*$ denotes the complex conjugate of $\{\cdots\}$.

The homogeneous strain, $\bar{\epsilon}_{ij}$, in (2) is the uniform macroscopic strain characterizing the macroscopic shape and volume change determined by the boundary constraint. If a boundary is constrained so that the system is not allowed to have any homogeneous deformation, the homogeneous strain, $\bar{\epsilon}_{ij}$, is equal to zero. Similarly, if a system is subject to an initial applied strain, $\epsilon^{\mathrm{a}}_{ij}$, and then the boundary is held fixed, $\bar{\epsilon}_{ij} = \epsilon^{\mathrm{a}}_{ij}$. On the other hand, if the system is stress-free, the homogeneous strain is obtained by minimizing the total elastic energy. In this work, for simplicity, we assume that the boundary is constrained so that $\bar{\epsilon}_{ij} = 0$.

The total elastic energy in (2) includes the homogeneous deformation energy of the system (the first term), the total coherency strain energy of a solid solution induced by a compositional inhomogeneity (the second and third terms), the strain energy of a structural defect (fourth and fifth terms), and the interaction energies among the homogeneous deformation, the coherency strain, and structural defects (the rest three terms). The corresponding Fourier transform of the elastic potential per atom involving both composition inhomogeneity and structural defects is given by

$$N_{\mathrm{v}}\mu_{\mathrm{el}}(\boldsymbol{g}) = \sigma^{\mathrm{o}}_{ij}\Big[\epsilon_{\mathrm{o}}\delta_{ij}\delta X(\boldsymbol{g}) + \epsilon^{\mathrm{d}}_{ij}(\boldsymbol{g})\Big] - n_i\sigma^{\mathrm{o}}_{ij}\Omega_{jk}(\boldsymbol{n})\big[\sigma^{\mathrm{o}}_{kl}\delta X(\boldsymbol{g}) + \sigma^{\mathrm{d}}_{kl}(\boldsymbol{g})\big]n_l, \tag{3}$$

where N_{v} is the number of atoms per unit volume.

3. Diffusion equation in the presence of compositional stress and defects

The interaction between composition and stress in general and the effect of compositional stress on diffusion in particular were extensively discussed by Larche and Cahn [3,26]. For a binary substitutional solid solution, the time-dependent Cahn–Hilliard diffusion equation is given by [3,26]

$$\frac{\mathrm{d}X(\boldsymbol{r})}{\mathrm{d}t} = \nabla\left[\frac{DX(1-X)}{k_{\mathrm{B}}T}\right]\nabla\left[\frac{\partial f_{\mathrm{inc}}(X)}{\partial X} - \kappa\nabla^2X + \mu_{\mathrm{el}}\right], \tag{4}$$

where $X(\boldsymbol{r})$ is the local composition, D is the solute diffusion coefficient in a dilute solution, k_{B} is the Boltzmann constant, T is temperature, $f_{\mathrm{inc}}(X)$ is the incoherent-free energy density of a solid solution, κ is the gradient energy coefficient [27], and μ_{el} is the elastic potential per atom. To avoid unnecessary discussions on numerical solutions to variable coefficient Cahn–Hilliard Eq. (4), we make a further simplification by assuming that the factor $X(1-X)$ is a constant given by $X_{\mathrm{o}}(1-X_{\mathrm{o}})$, where X_{o} is the overall composition.

Using the dimensionless units, $t^* = DtX_{\mathrm{o}}(1-X_{\mathrm{o}})/(\Delta x)^2$, $f^*_{\mathrm{inc}} = f_{\mathrm{inc}}/k_{\mathrm{B}}T$, $\mu^*_{\mathrm{el}} = \mu_{\mathrm{el}}/k_{\mathrm{B}}T$, $\nabla^* = (\Delta x)^2\nabla$, $r^* = r/\Delta x$, and $\kappa^* = \kappa/k_{\mathrm{B}}T(\Delta x)^2$, we have

$$\frac{\mathrm{d}X}{\mathrm{d}t^*} = (\nabla^*)^2\left[\frac{\mathrm{d}f^*_{\mathrm{inc}}(X)}{\mathrm{d}X} - \kappa^*(\nabla^*)^2X + \mu^*_{\mathrm{el}}\right]. \tag{5}$$

Taking a Fourier transform of both sides of Eq. (5), we have the temporal evolution of the composition wave amplitude, $X(\boldsymbol{g})$,

$$\frac{\mathrm{d}X(\boldsymbol{g}^*)}{\mathrm{d}t^*} = -(g^*)^2\left[\left(\frac{\mathrm{d}f^*_{\mathrm{inc}}(X)}{\mathrm{d}X}\right)_{g^*} + \kappa^*(g^*)^2X(\boldsymbol{g}^*) + \mu^*_{\mathrm{el}}(\boldsymbol{g}^*)\right], \tag{6}$$

where g^* is the magnitude of $\boldsymbol{g}^*$, $X(\boldsymbol{g}^*)$ and $\mu_{\mathrm{el}}(\boldsymbol{g}^*)$ are the Fourier transforms of $X(\boldsymbol{r}^*)$ and $\mu^*_{\mathrm{el}}(\boldsymbol{r}^*)$, respectively.

4. Eigenstrain $\epsilon^d_{ij}(\boldsymbol{r})$ for continuously distributed dislocations

A continuous distribution of dislocations can be described by a dislocation density tensor α_{ij}. The components of the jth row of the tensor are numerically equal to the components of the total Burgers vector of all dislocations crossing a unit area normal to the ith axis. Let there be n^k dislocations with a dislocation line direction θ^k passing through a unit area normal to θ^k and having Burgers vectors $\boldsymbol{b}^k$, then the dislocation density tensor is defined as [28],

$$\alpha_{ji} = \sum n^k \theta^k_j b^k_i = \sum \theta^k_j B^k_i, \tag{7}$$

where $\boldsymbol{B}^k = n^k \boldsymbol{b}^k$ is the total Burgers vector of n^k dislocations with the same Burgers vector $\boldsymbol{b}^k$. Let β_{ij} denotes the plastic distortion tensor, the eigenstrain is written as,

$$\epsilon^{\mathrm{d}}_{ij}(\boldsymbol{r}) = \frac{1}{2}[\beta_{ij}(\boldsymbol{r}) + \beta_{ji}(\boldsymbol{r})]. \tag{8}$$

For a given continuous distribution of dislocation α_{ij}, plastic distortion can be expressed in terms of Fourier coefficient of the dislocation density tensor $\alpha_{ij}(\boldsymbol{g})$ [2], namely,

$$\beta_{mn}(\boldsymbol{r}) = \varepsilon_{mlj} \int_{-\infty}^{+\infty} \frac{v_l}{i\boldsymbol{g}\cdot\boldsymbol{v}} \alpha_{jn}(\boldsymbol{g}) \exp(i\boldsymbol{g}\cdot\boldsymbol{r})\,\mathrm{d}\boldsymbol{g}, \tag{9}$$

where ε_{mlj} is the Levi–Civita tensor, $\boldsymbol{v}$ is the direction of dislocation motion, v_l is the lth component of $\boldsymbol{v}$. It should be pointed out that although the plastic distortion tensor β_{mn} depends on the choice of $\boldsymbol{v}$, the stress caused by the dislocations is unique, independent of the choice of $\boldsymbol{v}$. Performing the Fourier transforms of $\beta_{mn}(\boldsymbol{r})$, we get $\epsilon^{\mathrm{d}}_{kl}(\boldsymbol{g})$ in Eq. (3) for a given dislocation distribution,

$$\epsilon^{\mathrm{d}}_{kl}(\boldsymbol{g}) = \frac{1}{2}[\beta_{kl}(\boldsymbol{g}) + \beta_{lk}(\boldsymbol{g})] = \varepsilon_{kmj}\frac{v_m}{i\boldsymbol{g}\cdot\boldsymbol{v}}\alpha_{jl}(\boldsymbol{g}) + \varepsilon_{lmj}\frac{v_l}{i\boldsymbol{g}\cdot\boldsymbol{v}}\alpha_{kn}(\boldsymbol{g}). \tag{10}$$

Dislocations in crystals tend to form an equilibrium distribution under the combined action of their mutual interactions, the force acted on them by applied stresses, and frictional stresses. For instance, dislocations often pile up at grain boundaries, inclusions or other crystal defects which prevent them passing through. The model of dislocation pile-ups has been used reasonably to explain crack initiations [2] and phase nucleations [29]. On the other hand, a number of crystal defects, such as twins, grain boundaries, interfaces of incoherent particles, and cracks which induce deformation incompatibilities, can be described by continuously distributed dislocations. To illustrate how to construct the eigenstrain tensor for a given dislocation distribution, we consider two simple examples, i.e., slip bands and crack-like condensed interstitial dislocation loops, which can be described by a set of identical dislocations lying on the same plane ($y = 0$) with the dislocation line direction $\theta = (0, 0, 1)$ (see Fig. 1). Dislocations on the slip plane of slip band shown in Fig. 1(a), which has Burgers vector $\boldsymbol{b} = (\pm b_0, 0, 0)$, move under shear stress, pile up at the grain boundaries and form an equilibrium distribution of dislocations. By assuming the applied shear stress and frictional stress on the slip plane to be constant, and assuming the frictional stress at grain boundaries is large enough to hold back dislocation slipping, the equilibrium dislocation density on the slip plane ($y = 0$) can be described as [2],

$$D(x) = \frac{D_0 x}{(d^2 - x^2)^{1/2}}[H(x + d) - H(x - d)], \tag{11}$$

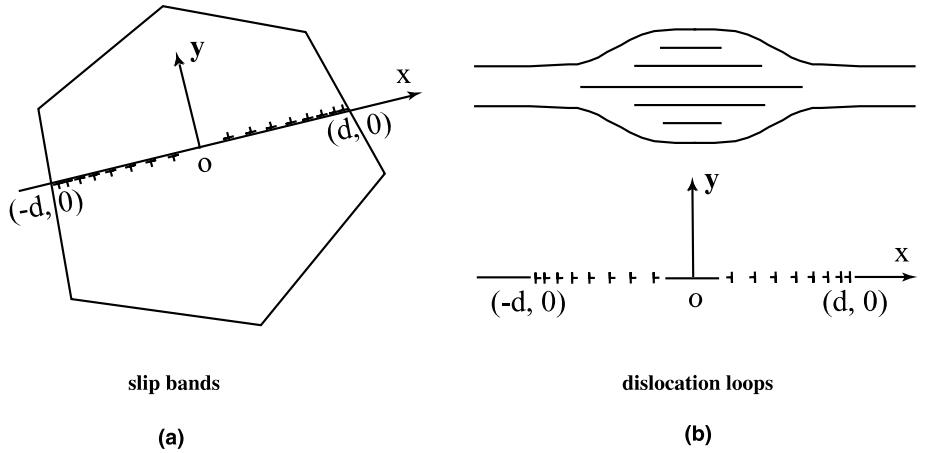

Fig. 1. Dislocation model of slip bands and dislocation loops.

where D_0 is a constant depending on the applied stress, frictional stress, elastic constant, and the Burgers vector, d is the pile-up length, as shown in Fig. 1(a), and $H(x)$ is the Heaviside step function. The Burgers vector associated with such a dislocation distribution is $\boldsymbol{B}(x,y) = (b_0 D(x)\delta(y), 0, 0)$, where $\delta(y)$ is the Dirac's delta function. The total number of dislocations piled up on the slip plane in the region $(0,d)$ is calculated by

$$N = \int_0^d D(x)\,\mathrm{d}x = D_0 d \tag{12}$$

and an equal number of negative ones piled up in the region $(-d,0)$. We choose the direction of dislocation movement, $\boldsymbol{v}$, to be (1, 0, 0). Then according to the definition of dislocation density tensor α_{ij}, we get

$$\alpha_{31}(x,y) = \frac{D_0 b_0 x}{(d^2 - x^2)^{1/2}}\delta(y)[H(x+d) - H(x-d)]. \tag{13}$$

Other components of the dislocation density tensor are zero. The corresponding eigenstrain of such a dislocation distribution is

$$\epsilon_{12}(x,y) = \epsilon_{21}(x,y) = D_0 b_0 (d^2 - x^2)^{1/2}\delta(y)[H(x+d) - H(x-d)], \tag{14}$$

where b_0 is the component of dislocation Burgers vector in x direction. The other components of eigenstrain tensor are zero. Fig. 2 shows the distribution of dislocation density $D(x)/D_0$ and eigenstrain $\epsilon_{12}/(D_0 b_0)$. We can find that the dislocation density is infinity and the eigenstrain tends to zero quickly at $x = \pm d$ where the stress field is singular. Fig. 1(b) presents crack-like condensed interstitial dislocation loops [28]. Assuming the applied stress and dislocation climbing force are constant, and choosing (1, 0, 0) as the direction of dislocation movement, the following dislocation density tensor gives the equilibrium dislocation distributions for the defect shown in Fig. 1(b).

$$\alpha_{32}(x,y) = \frac{D_0 b_0 x}{(d^2 - x^2)^{1/2}}\delta(y)[H(x+d) - (x-d)]. \tag{15}$$

Other components of the dislocation density tensor are zero. The eigenstrains associated with such a distributed dislocation loops are

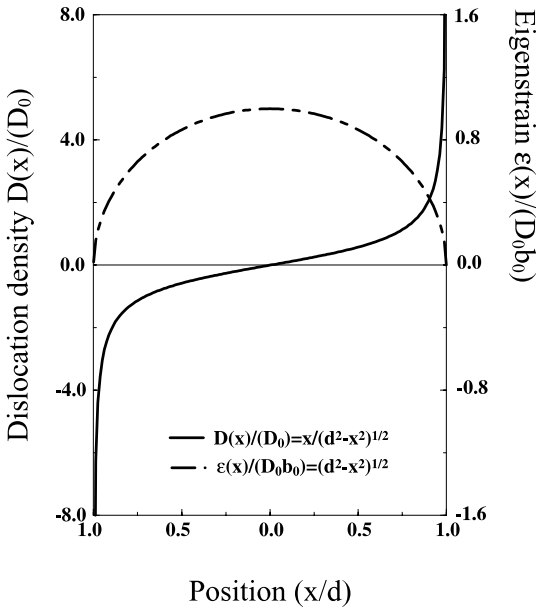

Fig. 2. Dislocation density $D(x)$ and eigenstrain $\epsilon_{22}(x) = \epsilon(x)$ for dislocation loops; $\epsilon_{12}(x) = \epsilon(x)$ for slip bands.

$$\epsilon_{22}(x,y) = D_0 b_0 (d^2 - x^2)^{1/2} \delta(y)[H(x+d) - H(x-d)]. \tag{16}$$

More complicated defects such as vacancy dipoles, interstitial dipoles, and cracks [2,28] can be described by combining dislocation density tensors (14) and (16). To study the role of distributed dislocations on solute segregation and phase transformation in real material, we need to extract a relative dislocation tensor α_{ij} from experimental observations.

5. Examples and Discussions

In the examples discussed below, we solved the diffusion Eq. (6) using a semi-implicit method [30],

$$X(\boldsymbol{g}^*, t^* + \Delta t^*) = \frac{X(\boldsymbol{g}^*, t) - \Delta t^* (g^*)^2 \left[\left(\frac{\mathrm{d}f^*_{\mathrm{inc}}(X)}{\mathrm{d}X} \right)_{\boldsymbol{g}^*} + \mu^*_{\mathrm{el}}(\boldsymbol{g}^*) \right]}{1 + \Delta t^* \kappa^* (g^*)^4}, \tag{17}$$

where Δt^* is the time step for integration. We use a small time step size of 0.05 for the initial 1000 time steps and then it is increased to 5.0. The elastic constants are chosen to make the system elastically isotropic with G (the shear modulus) and v (the poisson ratio) equal to 100 (in units of $N_v k_B T$) and 0.25, respectively. It should be pointed out that the same computer code can be used for elastically anisotropic systems without any modification. We use the following local coherent-free energy density at a given temperature,

$$f^*(X) = (X - 0.5)^2 [-1.0 + 2.5(X - 0.5)^2]. \tag{18}$$

It is a double-well free energy function as a function of composition. A single homogeneous solid solution is stable below $X_{\alpha'} = 0.053$ or above $X_{\alpha''} = 0.947$. The equilibrium state for intermediate compositions is a two-phase mixture with equilibrium compositions, $X_{\alpha'} = 0.053$ and $X_{\alpha''} = 0.947$, respectively. The spinodal

compositions, $X_{s'}$ and $X_{s''}$ are 0.242 and 0.758. The corresponding incoherent-free energy, $f^*_{\text{inc}}(X)$ is given by $f^*(X) + e_{\text{hom}}/(N_v k_B T)$, where e_{hom} is the elastic energy density of a homogeneous solid solution. For an isotropic solid solution in 2D,

$$e^{\text{iso}}_{\text{hom}} = \frac{G}{1-v}\epsilon_o^2 X(1-X). \tag{19}$$

The gradient coefficient is 1.0. We assumed that the composition expansion coefficient is positive with expansion coefficient 0.05. The Burgers vector, $\boldsymbol{b}$, is chosen to be (0.1, 0.0) for slip bands and (0.0, 0.1) for dislocation loops in unit of Δx with $\Delta x = 1.0$. All the numerical calculations presented below were performed in two dimensions and with the same parameters listed above.

5.1. Solute segregation around dislocation loops

As an example, solute segregation around distributed dislocation loops in 2D are considered in this section. We performed a numerical simulation using a 512×512 grid. The distributed dislocation loops is placed on a line of grid points between the coordinates (128, 256) and (384, 256) as shown in Fig. 3(a), and the dislocation line direction is along the normal to the 2D domain. The values of the eigenstrain calculated with Eq. (16) are assigned to the grid points occupied by dislocation loops. In the present paper the equilibrium dislocation distribution (Eq. (15)) under loading is employed, and dislocations do not move during solute diffusion. Experimental results show that equilibrium distribution of dislocations formed under loading usually remains the same during unloading [2]. The effect of internal stress on the equilibrium dislocation distribution will be discussed in a separated paper. The initial composition is uniform everywhere with a value of 0.03 which is outside the coherent two-phase field. We fix the dislocation pile-up length $d = 128$, and change D_0 to give different dislocation densities $N = 3, 6, 18$ where N denotes the total number of dislocations piled up in $(0, d)$. An example of temporal evolution of the composition profile along the horizontal line shown in Fig. 3 is plotted in Fig. 4 for the case $N = 18$. It can been found that the compositions near dislocation pile-ups reach their equilibrium values very quickly from an initially ho-

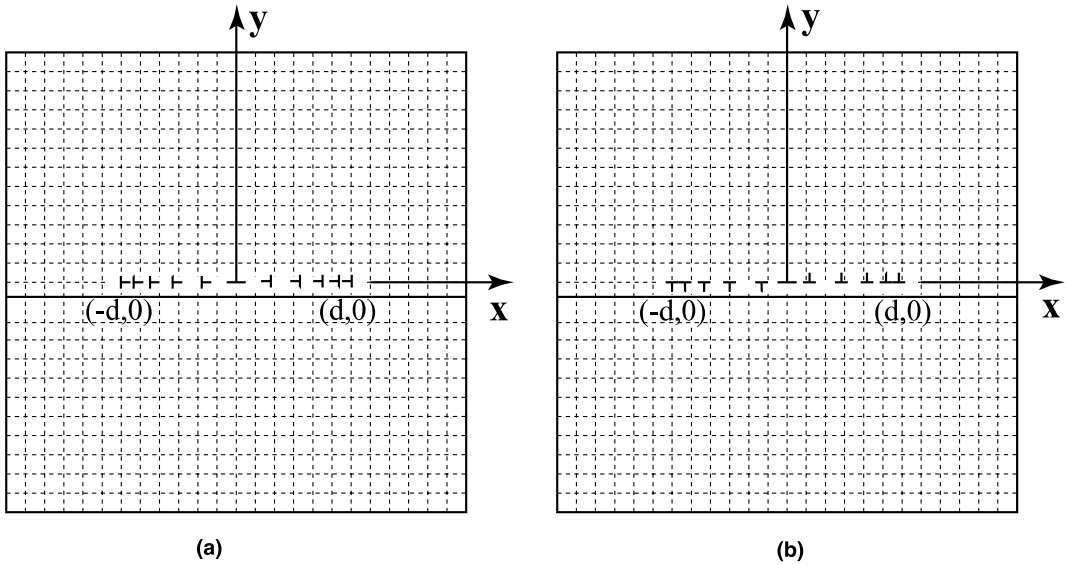

Fig. 3. Schematic representation of dislocation loops (a) and slip bands (b) in two dimension and a discretization grid.

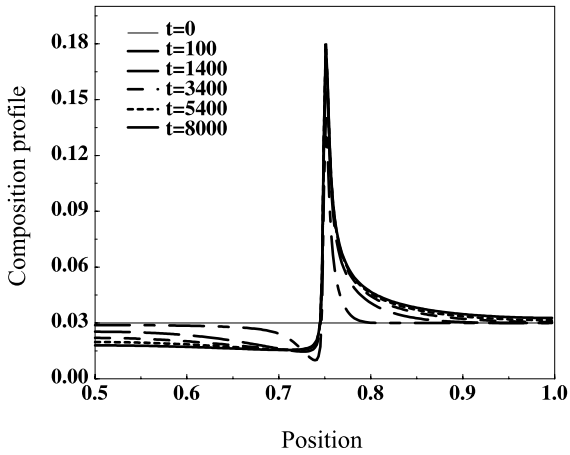

Fig. 4. Temporal evolution of the composition profiles along the horizontal line shown in Fig. 3 for the dislocation loops with 18 dislocations in $(0, d)$.

mogeneous solution driven by the strong stress inhomogeneity. The solute atoms simply diffuse from the compressive side to the tensile side of the dislocation. Fig. 5 presents the equilibrium composition profile around the dislocation loops at time step 8000. Different dislocation densities do not change the qualitative profile of solute segregation, but affect the maximum equilibrium compositions. The equilibrium composition profile as a function of dislocation density is shown in Fig. 6.

5.2. Nucleation and growth of precipitates around slip bands, and condensed interstitial dislocation loops

From the equilibrium dislocation distributions, we can find that a pile up of dislocations occurs at grain boundaries or obstacles ($x = \pm d$), where the dislocation density tends to infinity. As a result, a high stress concentration field is formed around dislocation pile-ups. As discussed in the previous section, such a high stress results in a solute segregation and depletion. Under certain circumstances, the degree of segregation is

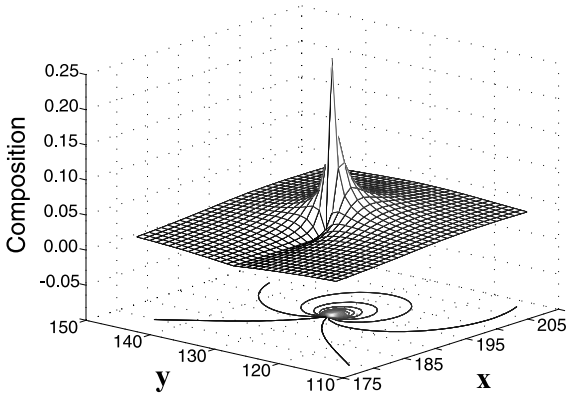

Fig. 5. The equilibrium composition profile around the dislocation pile-ups ($x = d$) for the dislocation loops.

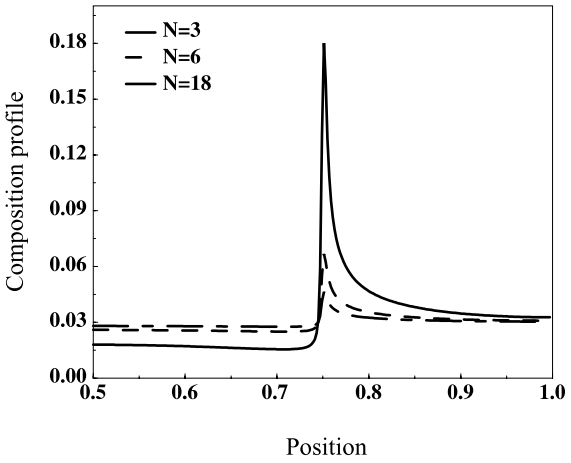

Fig. 6. The equilibrium composition profiles as a function of dislocation density along the horizontal line shown in Fig. 3 for the dislocation loops.

so high that nucleation and growth of a new phase around dislocation pile-ups occurs. To examine the nucleation and growth of a coherent precipitate induced by the stress field of slip bands and dislocation loops, we chose an average composition of 0.22 which is inside the coherent two-phase field, but outside the coherent spinodal region. We performed numerical simulations using the same simulation parameters as the solute segregation case above except the average composition. The slip bands and dislocation loops are introduced into the simulation cell by assigning grid points the eigenstrain value calculated with Eqs. (14) and (16), respectively. For the slip band with 18 dislocations in $(0, d)$, temporal evolution from homogeneous solution to nucleation and growth of precipitate is presented in Fig. 7. The black region in Fig. 7 represents the matrix with low composition while the white region represents the second-phase precipitate with high composition. Because the composition expansion coefficient of lattice parameter, ϵ_0, is assumed to be larger than zero, as expected, segregation of solutes takes place on the tensile side of the slip bands while depletion of solutes on the compressive side. Several nuclei with a composition close to the equilibrium composition started to form at time step 400 along the tensile side of the slip bands. The nucleus grow to a thin-long precipitate. Fig. 8(a) shows the effect of dislocation intensity ($N = 1$, 2, 3, 6, 12, 18) in the slip band on precipitate morphology. The composition profile along the horizontal line in Fig. 3 is shown in

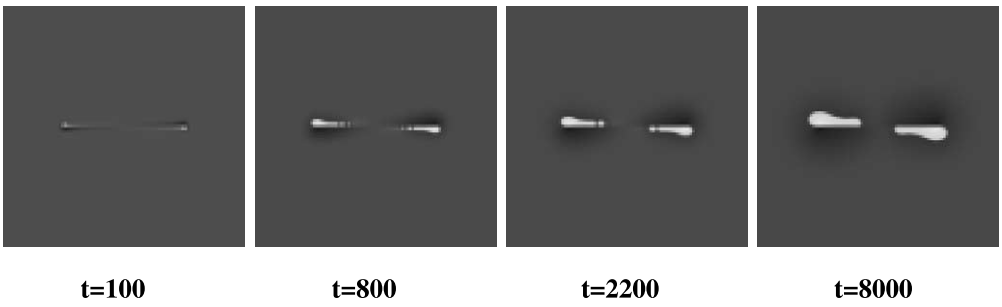

Fig. 7. Morphological evolution during nucleation, and growth of precipitates along the slip bands with 18 dislocations in $(0, d)$.

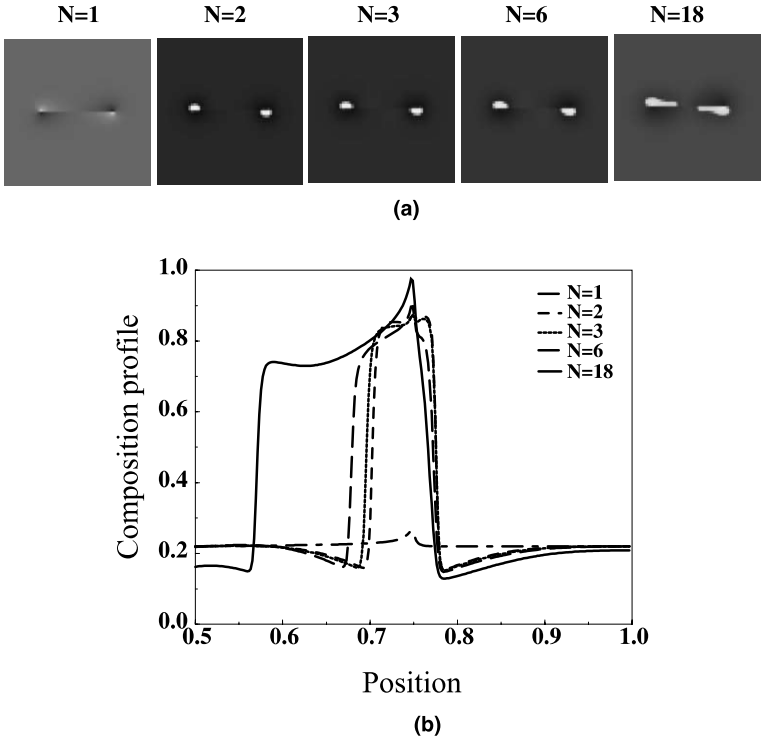

Fig. 8. (a) Precipitate morphology along the slip bands with different dislocation densities; (b) the equilibrium composition profiles along the horizontal line shown in Fig. 3 for the slip bands.

Fig. 8(b). We can find from the composition profile that the stress field of slip band with only a single dislocation causes solute segregation, but is not large enough to induce nucleation of a new phase. This is different from the results presented in our previous paper for a single dislocation located at one point. The reason is that the dislocation is spread out in a region $(0, d)$ in the present case which reduces the dislocation stress field. When the total number of dislocations is larger than two, the slip band stress field leads to precipitation of second-phase particles through a nucleation and growth mechanism. In addition, the morphologies of precipitates are dependent on the dislocation density of slip bands. Fig. 9(a) and (b) shows the dependence of precipitate morphology around dislocation loops on the dislocation density. In this case, precipitates form at $\pm d$ when $N > 2$. We can find that the precipitate morphologies are quite different for the two cases: slip bands and dislocation loops.

As discussed above, defect stress field may induce nucleation and growth of a new phase. Similarly, the formation of new phase may result in a change in the stress distribution and elastic properties, hence a change of material damage behavior. The proposed model in the present paper, cannot only be employed to simulate defect stress-induced phase transformation, but also be used to study the effect of phase transformation on mechanical properties. The advantage of this model compared with continuous mechanic models is that it avoids tracking individual dislocation segments and morphologies of phase transformation region. The average stress distributions caused by dislocations and lattice mismatch between new phase and parent phase along the horizontal line shown in Fig. 3 are plotted in Fig. 10. It can be found in both cases that the formation of precipitates decreases the tensile stress concentration caused by distributed dislocations. Of course, a quantitative analysis of the stress field, and precipitate nucleation and growth requires

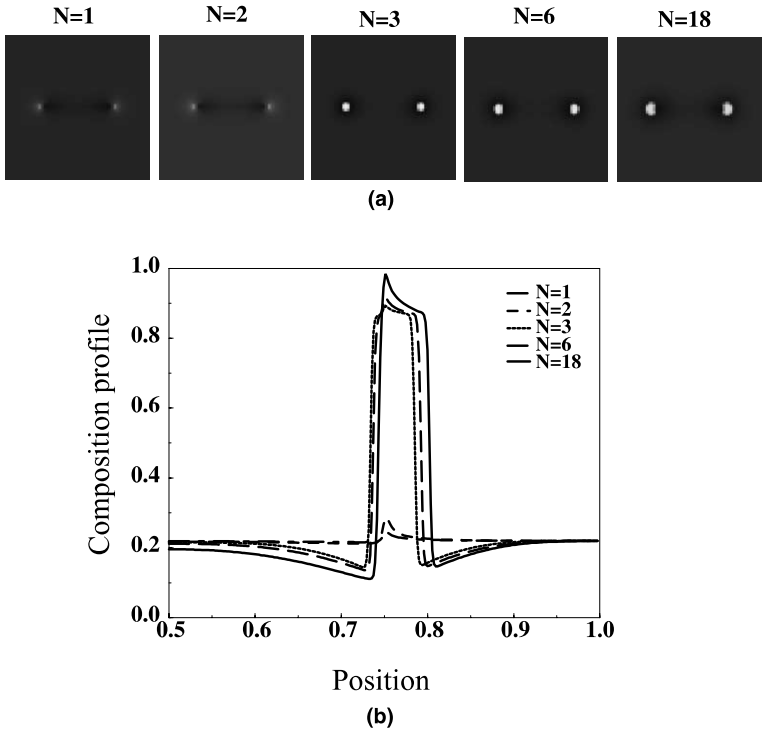

Fig. 9. (a) Precipitate morphology along the dislocation loops with different dislocation densities; (b) the equilibrium composition profiles along the horizontal line shown in Fig. 3 for the dislocation loops.

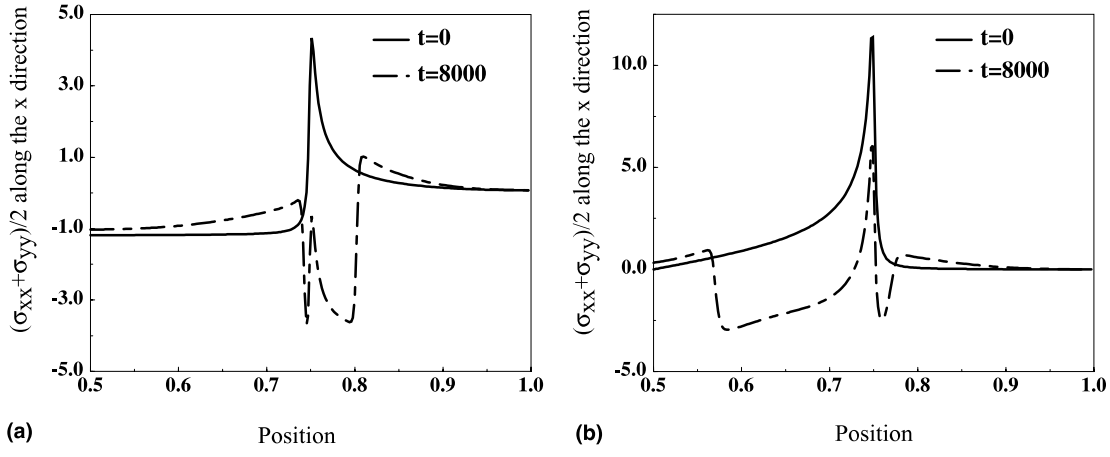

Fig. 10. The average stress distributions along the horizontal line shown in Fig. 3 before and after the formation of precipitates. (a) and (b) for the dislocation loops and slip bands with 18 dislocations, respectively.

real material parameters such as energetic barrier of nucleation, interface energy, mismatch eigenstrain, elastic constant, dislocation distribution and so on.

6. Summary

A diffuse-interface field model is proposed for predicting the morphological and microstructural evolution in coherent systems with arbitrary spatial distribution of structural defects such as grain boundary, mismatch inclusions, and dislocations. Within this model, the elastic stresses due to a compositional inhomogeneity and structural defects are solved consistently within the same formulation. We applied our model to solute segregation as well as to the nucleation and diffusional growth of a coherent precipitate around slip bands and condensed interstitial dislocation loops. It is shown that the coherent nucleation may become barrierless under the influence of the local elastic field of the dislocation distribution. The morphology of precipitate depends on defects and dislocation density.

Acknowledgements

The authors are grateful for the financial support from the NSF under the grant no. DMR-96-33719. The simulations were performed at the San Diego Supercomputer Center and the Pittsburgh Supercomputing Center.

References

[1] A.G. Khachaturyan, Theory of Structural Transformations in Solids, Wiley, New York, 1983.
[2] T. Mura, Micromechanics of Defects in Solids, Kluwer Academic Publishers, Dordrecht, 1987.
[3] F.C. Larche, J.W. Cahn, The interactions of composition and stress in crystalline solids, Acta metall. 33 (1985) 331–357.
[4] H. Nishimori, A. Onuki, Pattern formation in phase-separating alloys with cubic symmetry, Phys. Rev. B 42 (1990) 980–983.
[5] L.Q. Chen, Y.Z. Wang, A.G. Khachaturyan, Transformation-induced elastic strain effect on the precipitation kinetics of ordered intermetallics, Phil. Mag. Lett. 64 (1991) 241–251.
[6] Y. Wang, L.Q. Chen, A.G. Khachaturyan, Kinetics of strain-induced morphological transformation in cubic alloys with a miscibility gap, Acta Metall. Mater. 41 (1995) 279–296.
[7] T.A. Abinandanan, W.C. Johnson, Coarsening of elastically interacting coherent particles – theoretical formulations, Acta Metall. Mater. 41 (1993) 17–25.
[8] M.E. Thompson, C.S. Su, P.W. Voorhees, The equilibrium shape of a misfitting precipitate, Acta Metall. Mater. 42 (1994) 2107–2122.
[9] C. Sagui, A.M. Somoza, R. Desai, Spinodal decomposition in an order-disorder phase transition with elastic fields, Phys. Rev. E 50 (1994) 4865–4879.
[10] P. Fratzl, O. Penrose, Ising model for phase separation in alloys with anisotropic elastic interaction – I. theory, Acta Metall. Mater. 43 (1995) 2921–2930.
[11] T. Koyama, T. Miyazaki, A.E. Mebed, Computer simulation of phase decomposition in real alloy systems based on the khachaturyan diffusion equation, Metall. Mater. Trans. A 26 (1995) 2617–2623.
[12] J.K. Lee, A study on coherency strain and precipitate morphology via a discrete atom method, Metall. Mater. Trans. A 27 (1995) 1449–1459.
[13] H.J. Jou, P.H. Leo, J.S. Lowengrub, Microstructural evolution in inhomogeneous elastic solids, J. Comput. Phys. 131 (1997) 109–148.
[14] P. Fratzl, O. Penrose, J.L. Lebowitz, Modeling of phase separation in alloys with coherent elastic misfit, J. Stat. Phys. 95 (1999) 1429–1503.
[15] J.K. Lee, Dynamic interaction between a coherent precipitate and an edge dislocation, Metall. Mater. Trans. A 29 (1998) 2039–2048.
[16] J.M. Rickman, Y. Wang, D.J. Srolovitz, R. Lesar, Dislocation motion in the presence of diffusing solutes: A computer simulation study, Acta Mater. 48 (2000) 2163–2175.
[17] F. Léonard, R. Desai, Spinodal decomposition and dislocation lines in thin films and bulk materials, Phys. Rev. B 58 (1998) 8277–8288.
[18] J.W. Cahn, On spinodal decomposition, Acta Metall. 9 (1961) 795.
[19] S.Y. Hu, L.Q. Chen, Solute segregation and coherent nucleation and growth near a dislocation- a diffuse-interface model integrating defect and phase microstructures, Acta Mater. 49 (2001) 463–472.

[20] S. Kajiwara, Roles of dislocations and grain boundaries in martensite nucleation, Metall. Trans. A 17 (1985) 1693.
[21] J.E. Balley, Electron microscope observations on the precipitation of zirconium hydride in zirconium, Acta Met. 11 (1963) 267.
[22] N. Yoshikawa, H. Matsui, M. Koiwa, An in situ observation of hydrogen induced crack in niobium, Acta Met. 35 (1987) 413.
[23] H. Fujita, T. Katayama, In-situ observation of strain-induced $\gamma \rightarrow \epsilon \rightarrow \alpha'$ and $\gamma \rightarrow \alpha'$ martensitic transformations in Fe–Cr–Ni alloys, Mater. Trans. JIM 33 (1992) 243.
[24] A.A. Bulbich, Nucleation on the crack tip and transformation toughness in crystals undergoing structural phase transitions, J. Mater. Sci. 27 (1992) 1070.
[25] A.G. Kachaturyan, G.A. Shatalov, Elastic interaction potential of defects in a crystal, Sov. Phys. Solid State 11 (1969) 118.
[26] F.C. Larche, J.W. Cahn, The effect of self-stress on diffusion in solids, Acta Metall. 30 (1982) 1835–1845.
[27] J.W. Cahn, J.E. Hilliard, Free energy of a nonuniform system, i: Interfacial free energy, J. Chem. Phys. 28 (1958) 258.
[28] H. Liebowitz, Fracture, Academic press, New york, 1968.
[29] H. Nakamori, T. Furuhara, T. Maki, Crystallography of α phase precipitated on dislocations and deformation twin boundaries in a β titanium alloy, Crystallogr. Mater. Trans. JIM 33 (1992) 585–595.
[30] L.Q. Chen, J. Shen, Applications of semi-implicit Fourier-spectral method to phase-field equations, Comput. Phys. Commun. 108 (1998) 147–158.